Inequivalent Routes across the Mott Transition in V$_2$O$_3$ Explored by X-Ray Absorption

F. Rodolakis,[1,2] P. Hansmann,[3,4] J.-P. Rueff,[2,5] A. Toschi,[3] M. W. Haverkort,[4] G. Sangiovanni,[3] A. Tanaka,[6]
T. Saha-Dasgupta,[7] O. K. Andersen,[4] K. Held,[3] M. Sikora,[8] I. Alliot,[8,9] J.-P. Itié,[2] F. Baudelet,[2] P. Wzietek,[1]
P. Metcalf,[10] and M. Marsi[1]

[1]*Laboratoire de Physique des Solides, CNRS-UMR 8502, Université Paris-Sud, F-91405 Orsay, France*
[2]*Synchrotron SOLEIL, L'Orme des Merisiers, Saint-Aubin, BP 48, 91192 Gif-sur-Yvette Cedex, France*
[3]*Institut for Solid State Physics, Vienna University of Technology, 1040 Vienna, Austria*
[4]*Max-Planck-Institut für Festkörperforschung, Heisenbergstrasse 1, D-70569 Stuttgart, Germany*
[5]*Laboratoire de Chimie Physique-Matière et Rayonnement, CNRS-UMR 7614, Université Pierre et Marie Curie,
F-75005 Paris, France*
[6]*Department of Quantum Matter, ADSM, Hiroshima University, Higashi-Hiroshima 739-8530, Japan*
[7]*S.N. Bose Center for Basic Sciences, Salt Lake, Kolkata, India*
[8]*ESRF, 6 rue Jules Horowitz, BP 220, 38043 Grenoble Cedex, France*
[9]*CEA/DSM/INAC/NRS 17 avenue des Martyrs, 38000 Grenoble, France*
[10]*Department of Chemistry, Purdue University, West Lafayette, Indiana 47907, USA*
(Received 29 May 2009; published 25 January 2010)

The changes in the electronic structure of V$_2$O$_3$ across the metal-insulator transition induced by temperature, doping, and pressure are identified using high resolution x-ray absorption spectroscopy at the V pre-K edge. Contrary to what has been taken for granted so far, the metallic phase reached under pressure is shown to differ from the one obtained by changing doping or temperature. Using a novel computational scheme, we relate this effect to the role and occupancy of the a_{1g} orbitals. This finding unveils the inequivalence of different routes across the Mott transition in V$_2$O$_3$.

Some materials present metal-insulator transitions (MIT) without any changes in crystal structure or long-range magnetic order. These phenomena, known as Mott-Hubbard transitions, constitute a fundamental signature of strong electronic correlations. The physics emerging in the vicinity of these transitions is highly nontrivial and the properties of such materials depend on small changes in the electronic structure induced by external parameters [1,2]. Several features of the MIT have been successfully clarified by resorting to realistic many-body calculations [3]. Yet, contrary to common assumptions, a growing number of experimental facts are revealing that this physical process is also strongly dependent on the route followed through the MIT. Here we show this to be the case for vanadium sesquioxide (V$_2$O$_3$). The isostructural MIT in Cr-doped V$_2$O$_3$ is considered as the textbook example of a Mott transition, which occurs between a paramagnetic insulator (PI) and a paramagnetic metallic (PM) phase by changing doping level (x), temperature (T), or pressure (P) [4]. As such V$_2$O$_3$ has served as a test bed for many theoretical models [5–11] and a sustained experimental effort.

Among the different experimental methods recently employed to study the electronic properties of the Mott transition in Cr-doped V$_2$O$_3$ [12–15], x-ray absorption spectroscopy (XAS) has played a crucial role. It was the detailed investigation of the V $L_{2,3}$ absorption edges [16] that demonstrated the necessity of abandoning the simple one band, $S = 1/2$, model to obtain a realistic description of the changes in the electronic structure at the phase transition. XAS can also be performed at the V K edge in the hard x-ray range: in this case, the preedge will carry most of the physical information we are interested in, as it is predominantly due to $1s \rightarrow 3d$ transitions. The excitations in this spectral region are influenced by the core hole and should be considered to be of an excitonic nature. The advantages over the $L_{2,3}$ edge studies are (i) a more straightforward interpretation (due to the simple symmetry of the s core hole, the multiplet structure reveals a direct view on the d states), and (ii) the possibility of applying external pressure as diamond anvil cells are compatible with hard x-rays.

We used V K edge XAS to explore extensively the MIT in V$_2$O$_3$ by changing temperature, doping, and applying an external pressure. The pre-K edges were analyzed by a novel computational scheme combining local density approximation and dynamical mean field theory (LDA + DMFT) [17] with configuration interaction (CI) full multiplet ligand field calculations to interpret subtle differences at the PM-PI transition. This allowed us to (i) observe in detail the changes in the electronic excitations, providing also a direct estimate of the Hund's coupling J, (ii) analyze the physical properties of the PI and PM phase on both sides of the MIT, leading to the main result of our work, (iii) understand the difference between P, T or doping-induced transitions. This difference is mainly related to the occupancy of the a_{1g} orbitals, suggesting the existence of a new "pressure" pathway between PI and PM in the phase diagram.

The experiments were performed on the inelastic x-ray scattering (IXS) beam lines ID-26 and BM-30 at the

European Synchrotron Radiation Facility (ESRF). We used high quality samples of $(V_{1-x}Cr_x)_2O_3$ with various doping in the PM ($x = 0$) and PI phases ($x = 0.011$, and 0.028) at ambient conditions. The MIT was also crossed for the 0.011 doping by changing temperature and for the 0.028 doping by pressure. To obtain the best resolution, the XAS spectra were acquired in the so-called partial fluorescence yield (PFY) mode [18], monitoring the intensity of the V-$K\alpha$ ($2p \rightarrow 1s$) line as the incident energy is swept across the absorption edge. Compared to standard XAS, the PFY mode provides better resolved absorption spectra as these are partly free from core-hole lifetime broadening effect. The gain is particularly appreciable at the transition metal K preedges as the $1s$ core-hole is extremely short lived with respect to the $2p$ core-hole and the dipolar tail is strongly reduced. The V-$K\alpha$ line was measured with the help of a IXS spectrometer equipped with a Ge(331) spherically bent analyzer. For the temperature dependence, the crystals were mounted in a cryostat installed on the spectrometer. On the other hand, measuring the PFY mode turned out to be difficult under pressure because of the weak fluorescence signal in the pressure cell, and we opted for standard XAS measurements in transmission mode. To maximize the throughput, a powder sample ($x = 0.028$) was loaded in a diamond anvil cell equipped with composite anvils made of a perforated diamond capped with a 500-μm thin diamond anvil. Pressure was measured *in situ* by standard ruby fluorescence technique. We used silicon oil as a pressure transmitting medium.

The T-dependent absorption spectra are displayed in Fig. 1(a) for both PM (200 K) and PI (300 K) phases for the $x = 0.011$, powder sample. The spectra have been normalized to an edge jump of unity. We will focus on the preedge region, where information about the V d states can be easier extracted. It can be decomposed into three spectral features (A, B, C) which all vary in intensity as the system is driven through the MIT whereas only C is considerably broadened [Fig. 1(a), inset]. Notice that no feature is observed below peak A contrary to the early results of Ref. [19] but in agreement with the more recent data of Ref. [20]. Within a simplified atomiclike picture, one could directly relate the intensity of features A, B, and C to the unoccupied states. Starting from a V-t_{2g}^2, $S = 1$ configuration, one can either add an electron to the t_{2g} subshell [split into one a_{1g} and two e_g^π states under trigonal distortion of the V sites [21] as shown in Fig. 1(d)] yielding peaks A and B, or add an electron to the e_g^σ subshell which gives rise to the broader peak C. In this picture, one could associate peak A with a spin quartet ($S = 3/2$) and peak B with a spin doublet ($S = 1/2$), split by the Hund's rule exchange.

This picture is, however, oversimplified as the V d electrons are strongly correlated and the spectra are still largely influenced by the $1s$ core-hole potential. Keeping that in mind, we have simulated the preedge by combining CI with LDA + DMFT calculations for which the one
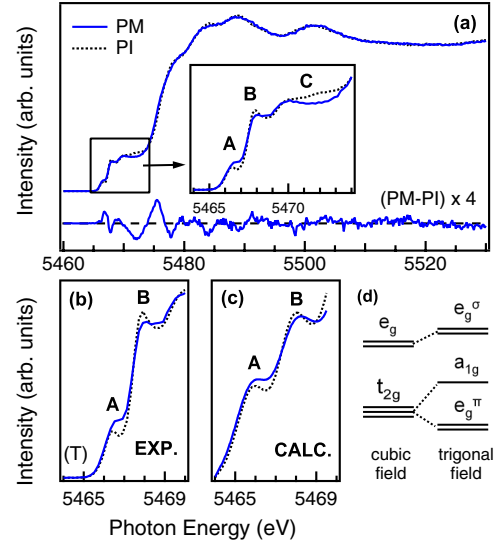

FIG. 1 (color online).   (a) V K edge x-ray absorption spectra in $(V_{1-x}Cr_x)_2O_3$, $x = 0.011$ powder sample measured as a function of temperature (T) in the PM (200 K, solid line) and PI (300 K, dotted line) phases by PFY XAS; below, PM-PI spectral difference; (inset) preedge region. (c) Calculated isotropic CI V K edge PM and PI spectra of V_2O_3. The spectra are compared to the T-dependent experimental data shown in the same energy window (b). (d) From LDA (starting point for our LDA + DMFT and CI calculations) we obtain that the cubic part of the ligand field splits the V d levels in t_{2g} and e_g by $10Dq \sim$ 2 eV, and that the small trigonal distortion further separates the t_{2g} into a_{1g} and e_g^π by $\Delta_{trig} \sim 0.3$ eV.

particle part (LDA) input corresponds to the level diagram in Fig. 1(d). We concentrate our analysis to peaks A and B, since peak C relates mainly to the unoccupied e_g^σ orbitals. These hybridize much stronger with the oxygen ligands and thus lack direct information on the Mott transition; peak C may also be related to nonlocal excitations (not included here) [22] which sensitively depend on the metal-ligand distance. Let us also note that the V sites in V_2O_3 are noncentrosymmetric which leads to an on-site mixing of V-$3d$ and V-$4p$ orbitals and interference between dipole and quadrupole transitions [7], included in our scheme.

Our CI calculations confirm that for the ground state the occupancy ratio between the (e_g^π, a_{1g}) and (e_g^π, e_g^π) states is smaller in the PI than in the PM phase [8,16]: the isotropic CI-based calculated XAS spectra in the preedge region reported in Fig. 1(c) agree well with the experimental data for both the energy splitting of features A and B and the ratio of their spectral weight (SW) which increases in the PM phase.

Considerable insight can be gained by comparing CI and LDA + DMFT calculations. Our LDA + DMFT calculations, performed using Nth-order muffin-tin orbital (NMTO) downfolded Hamiltonian for the 1.1% Cr-doped V_2O_3 and Hirsch-Fye quantum Monte Carlo method as impurity solver, confirm the above mentioned tendency

[we obtain a mixing of 50:50 and 35:65 for the (e_g^π, a_{1g}): (e_g^π, e_g^π) occupation in the PM and PI phases]. For LDA + DMFT we have chosen the same interaction parameter $U = 4.2$ eV for the PI phase as in Ref. [9] and followed their suggestion to slightly decrease its value in the PM phase (we assume $U = 4.0$ eV) [23]. Remarkably the simple structure of the core-hole potential in the K edge spectroscopy allows us to associate the preedge spectrum with the k-integrated spectral function above the Fermi energy calculated by LDA + DMFT. The electron-addition part of the spectral function shows three main features in PM phase: a coherent excitation at the Fermi level and a double peak associated to the incoherent electronic excitations, i.e., the upper Hubbard band (UHB), similarly to the undoped compound. In the PI phase obviously, only the latter survives. Comparison with the experimental spectra clearly shows that the preedge features have to be related to the "incoherent" part of the spectral function only. The physical reason is that the core-hole potential localizes the electrons destroying the coherent quasiparticle excitations and making the XAS spectrum atomiclike. All the "incoherent" LDA + DMFT, CI, and experimental spectra shown in Fig. 2 agree in many aspects, especially as for the splitting of the first two peaks by ≈ 2.0 eV (≈ 1.8 eV in experiment) which originates in LDA + DMFT from the Hund's exchange J in the Kanamori Hamiltonian. This further validates the choice of $J = 0.7$ eV used in our calculations contrasting with larger values assumed in previous studies [8,10,23], and also clarifies the mismatch between XAS and LDA + DMFT spectra reported in the undoped V_2O_3 compound [8]. Moreover, the ratio between A and B peak displays the same trend in the PM-PI transition as the CI (or experimental) data. The quantitative difference between the two

calculations is attributed to the lack of matrix elements in LDA + DMFT.

The intensity ratio of the first two incoherent excitations peaks A and B (associated to the quartet and doublet states in the oversimplified picture) thus appears as the key spectral parameter to understand the differences between PM and PI. Even in a powder sample, this ratio is still sensitive to the a_{1g} orbital occupation of the initial state. Indeed, due to the trigonal distortion a considerable spectral weight transfer from the peak B to higher energies (corresponding to final states with two a_{1g} electrons in the limit of large Δ_{trig}) can take place for the (e_g^π, a_{1g}) but not for the (e_g^π, e_g^π) initial state. Therefore, the K preedge XAS can serve as a direct probe of the a_{1g} orbital occupation in the ground state. As a rule of thumb, the larger the ratio between the SW of A and B, the larger the a_{1g} orbital occupation.

Hard x-ray absorption also provides a unique way to explore the "pressure" pathway across the MIT, from which relevant information can be extracted by applying our interpretation scheme. Figure 3(a) shows the XAS powder spectra of the P-induced MIT with the corresponding spectra for the T- and doping-driven transition (cf. the loci in the phase diagram, Fig. 3). To ease the comparison, the pressure data set (P) obtained in transmission mode has been deconvolved from the $1s$ Lorentzian lifetime broadening (1 eV FWHM) using the GNXAS code [26] to match the improved resolution of data sets (x) and (T) measured by PFY-XAS. Together with the PM-PI differences in Fig. 3(b), Fig. 3(a) clearly evidences that, besides a rigid shift of the first two peaks of $\sim + 0.13$ eV and contrary to the doping- or T-driven transition, very small changes in spectral shapes and weights are observed in the P-driven MIT. In the light of the arguments discussed above, our finding proves that the metallic state reached by applying pressure is characterized by a much lower occupation of the a_{1g} orbitals compared to the metallic state reached just by changing temperature or doping. Importantly, the spectra measured through the doping-induced MIT are identical within the experimental uncertainty to those measured through the T-driven transition. The temperature-doping equivalence is confirmed by our photoemission data displayed in Figs. 3(c) and 3(d) [15] and is consistent with the very similar lattice parameter changes across the transition [27]. The x and T equivalence is also borne out by the observation from XAS at the L edges in doped V_2O_3 [16] that the a_{1g} occupation within both the PM or PI phases is mostly independent of the doping level. Hence, the local incoherent excitations probed by XAS at the V L edge or K preedge are not directly affected by disorder [28].

Our finding clearly shows the limits of the common assumption that temperature- or doping- and pressure-driven MIT in V_2O_3 can be equivalently described within the same phase diagram [27,29]. Indeed, the two different PM electronic structures that we observed reflect different
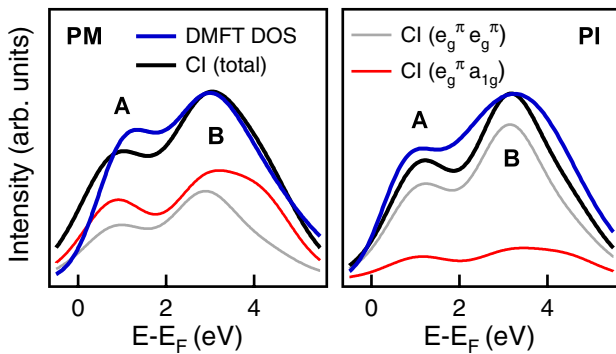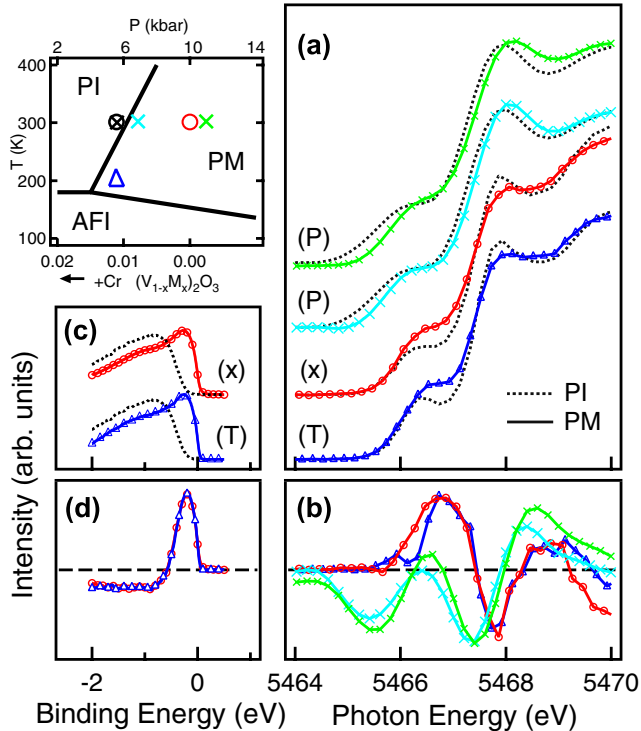

FIG. 2 (color online). Incoherent LDA + DMFT and CI calculations in the preedge region; E_F is the Fermi energy. Note the similarity in the main spectral features when crossing the MIT. Also shown are the different contributions of the CI spectrum labeled accordingly to their initial state: the contribution of the $(e_g^\pi, a_{1g}) \rightarrow (e_g^\pi, e_g^\pi, a_{1g})$ transitions to the peak $A(B)$ is approximately 60% (55%) in the PM phase and 20% (15%) in the PI phase.

FIG. 3 (color online). (a) V-*K* XAS spectra for powder samples of $(V_{1-x}Cr_x)_2O_3$ as a function of pressure ($\times$) [$x = 0.028$; 5 and 7 kbar (lower curves); 5 and 11 kbar (upper curves)] (*P*), temperature ($\triangle$) [$x = 0.011$; 200,300 K] (*T*), and doping ($\bigcirc$) [$x = 0, 0.011$] (*x*) (cf. points in the phase diagram; the pressure scale refers to the $x = 0.028$ doping). The spectral differences PM-PI ($\times 3$) shown for the three data sets (b) demonstrate the nonequivalence between *P* and temperature doping. The *x-T* equivalence is confirmed by the photoemission spectra ($h\nu = 9$ eV) (c) and their spectral differences (d) (from Ref. [15]).

mechanisms driving the MIT along different pathways. In the doping-driven MIT, the metallic phase is characterized by an increased occupation of the a_{1g} electrons indicating a reduced "effective crystal-field splitting" as the main driving mechanism towards metallicity [8,9], related to the jump of the lattice parameter c/a (1.4%) at the MIT [27]. In contrast, when pressure is applied the a_{1g} occupation remains basically unchanged, so that this metallic phase seems to originate rather from an increased bandwidth, without any relevant changes of the orbital splitting. The smaller c/a jump observed under pressure (0.7%) corroborates our analysis.

In conclusion, doping, temperature, and pressure are shown to act differently on the interplay between electron correlations and crystal field, so that states previously considered to be equivalent metals are actually different.

We believe this finding may apply to many other strongly correlated systems presenting metal-insulator transitions, with pressure opening inequivalent pathways through their phase diagrams.

[1] M. Imada, A. Fujimori, and Y. Tokura, Rev. Mod. Phys. **70**, 1039 (1998).
[2] E. Dagotto, Science **309**, 257 (2005).
[3] A. Georges *et al.*, Rev. Mod. Phys. **68**, 13 (1996).
[4] D. B. McWhan *et al.*, Phys. Rev. B **7**, 1920 (1973).
[5] C. Castellani, C. R. Natoli, and J. Ranninger, Phys. Rev. B **18**, 4945 (1978).
[6] K. Held *et al.*, Int. J. Mod. Phys. B **15**, 2611 (2001).
[7] I. S. Elfimov *et al.*, Phys. Rev. Lett. **88**, 015504 (2001).
[8] G. Keller *et al.*, Phys. Rev. B **70**, 205116 (2004).
[9] A. I. Poteryaev *et al.*, Phys. Rev. B **76**, 085127 (2007).
[10] M. S. Laad, L. Craco, and E. Muller-Hartmann, Phys. Rev. B **73**, 045109 (2006).
[11] A. Tanaka, J. Phys. Soc. Jpn. **71**, 1091 (2002).
[12] P. Limelette *et al.*, Science **302**, 89 (2003).
[13] S.-K. Mo *et al.*, Phys. Rev. Lett. **90**, 186403 (2003).
[14] S.-K. Mo *et al.*, Phys. Rev. B **74**, 165101 (2006).
[15] F. Rodolakis *et al.*, Phys. Rev. Lett. **102**, 066805 (2009).
[16] J.-H. Park *et al.*, Phys. Rev. B **61**, 11506 (2000).
[17] K. Held, Adv. Phys. **56**, 829 (2007).
[18] F. M. F. de Groot, Chem. Rev. **101**, 1779 (2001).
[19] A. Bianconi and C. R. Natoli, Solid State Commun. **27**, 1177 (1978).
[20] J. Goulon *et al.*, Phys. Rev. Lett. **85**, 4385 (2000).
[21] T. Saha-Dasgupta *et al.*, arXiv:0907.2841.
[22] C. Gougoussis *et al.*, Phys. Rev. B **79**, 045118 (2009).
[23] Constrained LDA/LDA + U estimates of *J* (0.93 eV in [24]) need to be reduced to $J \sim 0.7$ eV to reproduce the constrained LDA energy splitting with the DMFT Hamiltonian [17]. Moreover, the value of U adopted for LDA + U (2.8 eV) has to be assumed smaller than that for LDA + DMFT to compensate deficiencies of LDA + U [25].
[24] I. Solovyev, N. Hamada, and K. Terakura, Phys. Rev. B **53**, 7158 (1996).
[25] G. Sangiovanni *et al.*, Phys. Rev. B **73**, 205121 (2006).
[26] A. Filipponi, J. Phys. B **33**, 2835 (2000).
[27] D. B. McWhan and J. P. Remeika, Phys. Rev. B **2**, 3734 (1970).
[28] A. I. Frenkel *et al.*, Phys. Rev. Lett. **97**, 195502 (2006).
[29] An early version of the phase diagram (Fig. 15 in Ref. [27]) was drawn with a third pressure axis: due to the idea of *P-x* equivalence, this was later abandoned.